Earth and Planetary Science Letters 602 (2023) 117926

Contents lists available at ScienceDirect

Earth and Planetary Science Letters

journal homepage: www.elsevier.com/locate/epsl

Mercury isotope evidence for protracted North Atlantic magmatism during the Paleocene-Eocene Thermal Maximum

Simin Jin [a], David B. Kemp [a,*], Runsheng Yin [b], Ruiyang Sun [b], Jun Shen [c], David W. Jolley [d], Manuel Vieira [e,f], Chunju Huang [a]

[a] State Key Laboratory of Biogeology and Environmental Geology and Hubei Key Laboratory of Critical Zone Evolution, School of Earth Sciences, China University of Geosciences, Wuhan 430074, China
[b] State Key Laboratory of Ore Deposit Geochemistry, Institute of Geochemistry, Chinese Academy of Sciences, Guiyang 550081, China
[c] State Key Laboratory of Geological Processes and Mineral Resources, China University of Geosciences, Wuhan, Hubei, 430074, China
[d] Department of Geology & Geophysics, School of Geosciences, University of Aberdeen, King's College, Aberdeen, AB24 3UE, UK
[e] GEOBIOTEC, Department of Earth Sciences, NOVA School of Science and Technology, Campus de Caparica, P-2829 516 Caparica, Portugal
[f] Aker BP ASA., Strandveien 4, 1366 Lysaker, Oslo, Norway

ARTICLE INFO

Article history:
Received 26 August 2022
Received in revised form 16 November 2022
Accepted 17 November 2022
Available online 29 November 2022
Editor: A. Jacobson

Keywords:
PETM
North Atlantic Igneous Province
basaltic volcanism
mercury
mercury isotopes
large igneous province

ABSTRACT

The Paleocene-Eocene Thermal Maximum (PETM, ~56 Ma) was a major hyperthermal event that has been linked to CO_2 release from the North Atlantic Igneous Province (NAIP). Anomalously high sedimentary mercury (Hg) concentrations, a proxy for volcanism, have been recorded across the PETM, but the precise mechanistic links between NAIP emplacement and the event are unclear. Here, we present Hg abundance and Hg-isotope data across a thick, deep-marine sedimentary record deposited in close proximity to active NAIP volcanism. A marked transient shift of Δ^{199}Hg towards higher values occurs within the PETM onset, indicating a causal link to extrusive volcanic activity from the NAIP. Increasing Δ^{199}Hg values through the body of the PETM indicate a protracted interval of magmatism. Towards the end of, and after, the PETM the data suggest an overall waning influence of direct volcanogenic Hg outgassing. Our data can explain both the triggering mechanism and long duration of the PETM.

1. Introduction

Large igneous province (LIP) eruptions were a key driver of multiple mass extinctions throughout the Phanerozoic (e.g., Bond and Grasby, 2017). Magmatism from the North Atlantic Igneous Province (NAIP) initiated during the Paleocene and occurred in two main pulses divided by the opening of the North Atlantic Ocean (Wilkinson et al., 2017 and references therein). The second phase (dated to *ca*. 57-54 Ma) was associated with voluminous extrusive volcanism with subaerial lava flows expressed as seaward-dipping reflector sequences in Greenland, the Faroe Islands and Northern Ireland (Saunders et al., 1997; Wilkinson et al., 2017; Jolley et al., 2021). Geochronological data suggest peak magma production rates increased by an order of magnitude at 55.8 Ma (Storey et al., 2007; Schofield et al., 2018; Jolley et al., 2021; Kasbohm et al., 2021), broadly coincident with the Paleocene-Eocene thermal maximum (PETM, ~56 Ma). The PETM was the most significant hyperthermal of the Cenozoic, and was associated with seawater warming of 5-8 °C (Zachos et al., 2003; Sluijs et al., 2007), extinction of deep-sea benthic foraminifera (Thomas, 1989), increased atmospheric CO_2 (Gutjahr et al., 2017), ocean acidification (Zachos et al., 2005) and enhanced continental weathering (Dickson et al., 2015). In sedimentary strata worldwide, the PETM is characterized by a >2‰ negative carbon-isotope excursion (CIE), indicating an injection of ^{12}C-enriched carbon into the biosphere (Dickens et al., 1995; Svensen et al., 2004; Gutjahr et al., 2017).

Proposed triggers for the PETM include the destabilization of methane hydrates (Dickens et al., 1995), and/or large-scale volcanism (Svensen et al., 2004, 2010; Gutjahr et al., 2017). In recent years, geochemical and modeling evidence has suggested that the ^{12}C-enriched carbon released at the PETM was largely volcanogenic and sourced from the NAIP (Penman et al., 2014; Dickson et al., 2015; Gutjahr et al., 2017; Jones et al., 2019; Stokke et al., 2020). In addition, thousands of hydrothermal vent complexes have been identified on seismic reflection profiles in the Norwegian Sea, and it has been suggested that intrusion of NAIP mantle-derived melts into organic-rich sediments triggered the release of thermogenic

* Corresponding author.
E-mail address: davidkemp@cug.edu.cn (D.B. Kemp).

https://doi.org/10.1016/j.epsl.2022.117926
0012-821X/

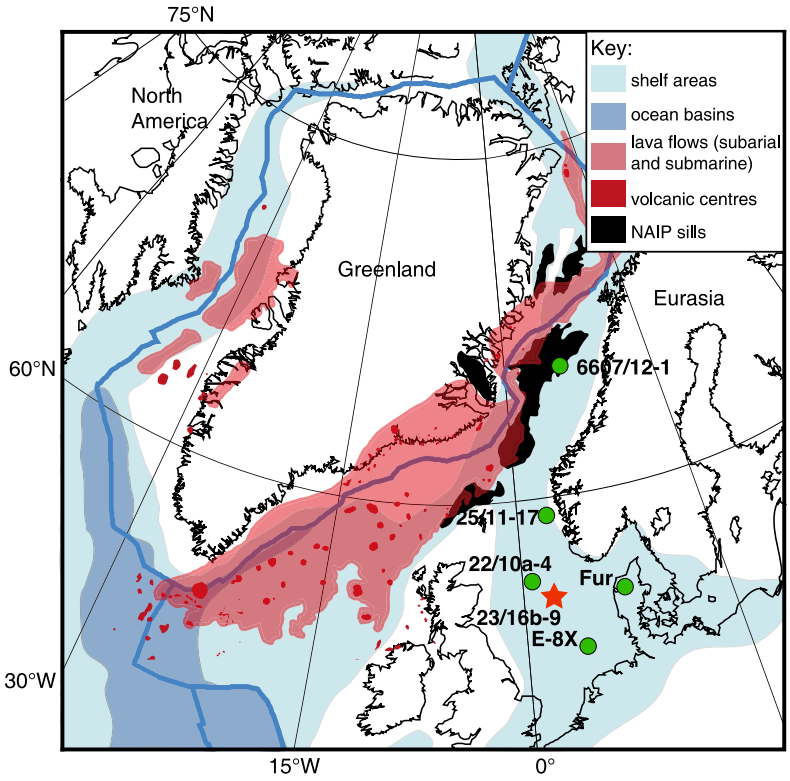

Fig. 1. Regional map of the location of the North Atlantic Igneous Province (NAIP) at 56 Ma. Also shown is the study site: well 23/16b-9 (red star). Other North Sea sites discussed in the text are shown with green dots. Modified from Jones et al. (2019) and Stokke et al. (2020). (For interpretation of the colors in the figure(s), the reader is referred to the web version of this article.)

methane, thus acting as a key contributory driver of the PETM (Svensen et al., 2004, 2010; Frieling et al., 2016).

Mercury (Hg) in sedimentary rocks is an emerging tool suitable for tracing ancient large-scale volcanism (Sanei et al., 2012; Thibodeau et al., 2016; Grasby et al., 2019; Shen et al., 2020). Volcanism is the primary natural Hg supply to Earth's surface system (Pyle and Mather, 2003; Selin, 2009). Since Hg in sediments and sedimentary rocks is mainly hosted by organic matter, sulfide minerals and clays, Hg is commonly normalized to total organic carbon (TOC), total sulfur (TS) and aluminum (Al, Ravichandran, 2004; Shen et al., 2020). The normalized values can aid in the recognition of anomalous Hg concentrations that are indicative of sourcing from large volcanic emissions, regardless of host phase abundance variations (Sanei et al., 2012; Grasby et al., 2019; Charbonnier et al., 2017; Percival et al., 2018; Shen et al., 2019a, 2019b, 2020).

Previous work on Hg concentrations and Hg/TOC ratios across the PETM has highlighted large variations (Keller et al., 2018; Jones et al., 2019; Liu et al., 2019; Kender et al., 2021; Tremblin et al., 2022). Spatially, Hg and Hg/TOC within, or just prior to, the PETM, are generally higher in areas close to the NAIP, such as in the North Sea Basin, Svalbard and Spain, supporting a link between the event and volcanism (Jones et al., 2019; Tremblin et al., 2022). However, in sections deposited far away from the NAIP, Hg contents and Hg/TOC ratios are generally lower, as is the case for samples from the New Jersey Coastal Plain (Jones et al., 2019; Liu et al., 2019). Hg-isotopes have the potential to yield detailed information on the sources and fluxes of Hg through events like the PETM beyond what can be inferred using Hg abundance data alone (Sial et al., 2016; Grasby et al., 2017; Shen et al., 2022a).

Mercury can undergo mass-dependent fractionation (MDF) and mass-independent fractionation (MIF) in nature (Bergquist and Blum, 2007). MDF of Hg generally provides only limited information on source as many processes can affect it, such as redox, biological activity and Hg phase changes (Blum et al., 2014). MIF of Hg in natural samples is mainly dominated by photoreduction of aqueous Hg^{II} to Hg^0, which leads to negative $\Delta^{199}Hg$ values of gaseous Hg^0 in the atmosphere, and positive $\Delta^{199}Hg$ values of soluble Hg^{II} in surface water and precipitation (Blum et al., 2014; Gratz et al., 2010). Gaseous Hg^0 with negative $\Delta^{199}Hg$ values in the atmosphere can then be taken up by plant foliage and buried in soil (Demers et al., 2013). As such, $\Delta^{199}Hg$ can indicate likely sources of Hg, yielding negative values in terrestrial materials (e.g., soils and vegetation) and positive values in the oceanic system from atmospheric wet precipitation (Blum et al., 2014). Importantly, Hg from direct modern volcanic emissions is expected to have $\Delta^{199}Hg$ of ~0‰ (Zambardi et al., 2009).

To date, only a single Hg-isotope datapoint has been presented across the PETM (Gleason et al., 2017). As such, the precise behavior and source of Hg across the PETM, and hence the mechanistic links between NAIP volcanism and the event, are still unknown. Here, Hg abundance and Hg-isotopes were analyzed for Paleocene-Eocene strata from well 23/16b-9 in the central North Sea Basin. The proximity of the well to the NAIP and the thickness make it an ideal site to explore and quantify signals of volcanic activity through the PETM interval.

2. Material and methods

2.1. Samples

Well 23/16b-9 is located in the central North Sea Basin (57°26′50.208″N, 02°08′27.624″E, Fig. 1). The studied succession comprises a thick, expanded record of mudstones and turbidite sandstones deposited in a deep-water fan system. Previous work has identified an extremely expanded record of the PETM carbon-isotope excursion (CIE) in this well (~140.2 m thick, Jin et al., 2022). A total of 122 samples from the 23/16b-9 well across the PETM were collected. The samples used in this study were a mix

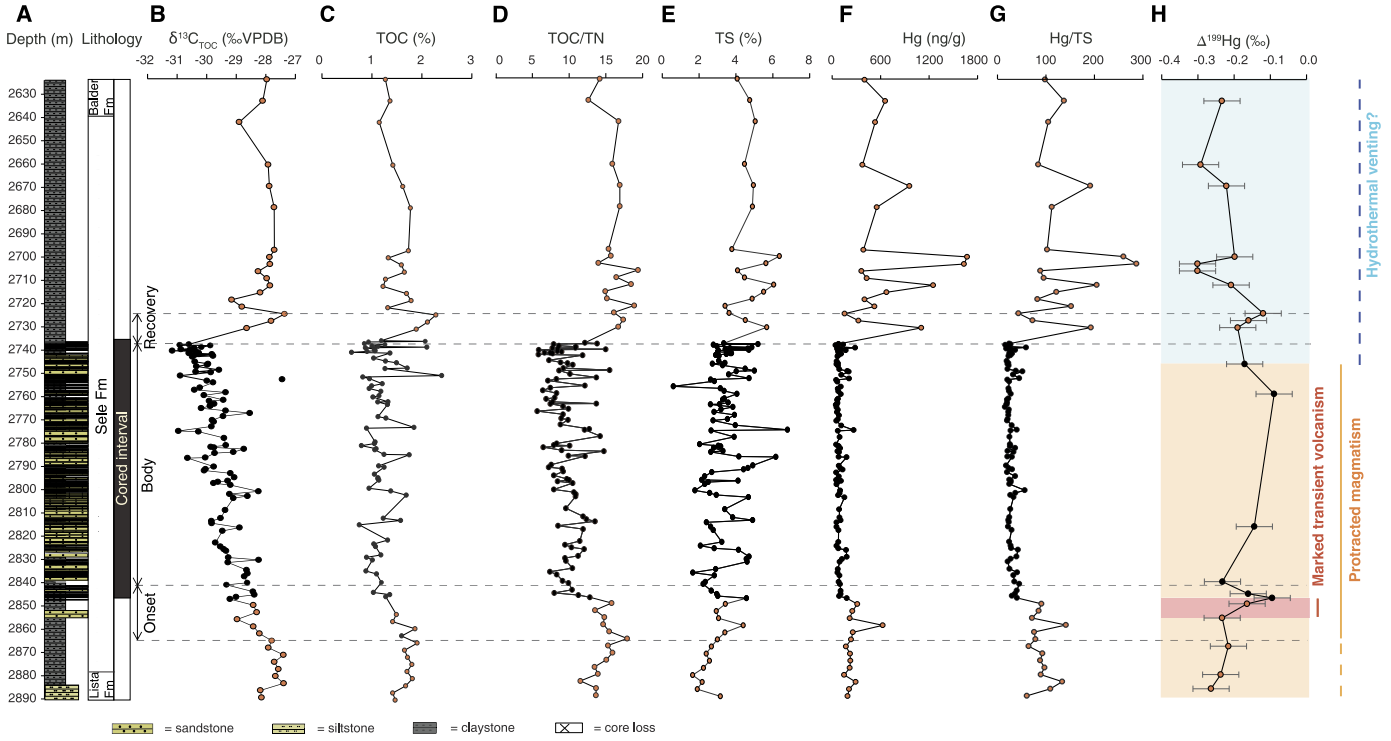

Fig. 2. Lithological and geochemical data through well 23/16b-9. (A) Lithostratigraphic log and formation names, as well as indication of cored interval. (B) Organic carbon-isotopes ($\delta^{13}C_{TOC}$, data from Jin et al., 2022), the isolated black point is an outlying value. (C) Weight percentage of total organic carbon (TOC, data from Jin et al., 2022). (D) Total organic carbon/total nitrogen ratio (TOC/TN). (E) Weight percentage of total sulfur (TS). (F) Hg concentration in ng/g. (G) Ratio of Hg to TS. (H) Mass-independent fractionation of odd Hg-isotopes (Δ^{199}Hg). For all plots, black points are from core samples taken from the cored interval of the well. Orange points are from wet cuttings samples. Dashed lines define the onset, body and recovery intervals of the PETM carbon-isotope excursion (CIE) based on the profile of organic carbon-isotopes measured on bulk sample as well as palynological residues (Jin et al., 2022).

of wet cuttings samples directly retrieved during the drilling operations, and core samples extracted from continuous core (32 wet cuttings samples, 90 core samples, Fig. 2). As the Sele Formation is a sand-dominated hydrocarbon reservoir, migrated hydrocarbons (which are generally more depleted in ^{13}C than the source kerogen, Stephenson et al., 2005) and residual drilling fluids pose a potential challenge for retrieving high quality and unaltered elemental and isotopic data from the rocks. Consequently, dichloromethane (DCM) washing was conducted on the 32 wet cuttings samples to de-oil them before all measurements. For further details see Jin et al. (2022).

2.2. Elemental analyses

All 122 samples were crushed to ~200 mesh in a Tungsten carbide mortar before geochemical analysis. Powdered samples were divided into several parts for sample pretreatment. All of the samples were decarbonated with 6 mol/L HCl and measured for total nitrogen (TN) content using a Vario MACRO Cube elemental analyzer (the same analysis yielded the TOC data previously published in Jin et al., 2022). Precision of the TN measurements was ±0.04% (weight %, 2 standard deviation). 121 samples were analyzed for major element abundances (Al and TS) using X-ray fluorescence (PANalytical PW2424 XRF spectrometer). Precision of the Al measurements was ±0.36% (2 standard deviation). Analytical precision of TS (2σ) was ±0.12%. Data accuracy of the XRF-measured TS data was ensured by calibrating the data using a subset of samples measured on a Vario MACRO Cube elemental analyzer.

2.3. Mercury concentrations and isotopes

Hg content was measured in 122 samples at both Yale University using a Direct Mercury Analyzer (DMA-80) (60 samples) and China University of Geosciences-Wuhan using a DMA-80 Evo (62 samples). Data quality from Yale University was monitored via multiple analyses of the MESS-3 standard, yielding an analytical precision (2σ) of ±0.4 ng/g of the Hg content. Data quality from CUG (Wuhan) was monitored via multiple analyses of the GBW07423 standard, yielding an analytical precision (2σ) of ±2 ng/g for Hg content. To investigate the potential effect of DCM-washing on the Hg content of cuttings samples (see Section 2.1, above), DCM-washing was conducted on 16 decarbonated core samples in order to specifically isolate any differences in Hg related to the washing procedure (Fig. S1).

Hg-isotope measurements were conducted on a subset of 21 samples. The extraction of Hg was conducted through a double-stage tube furnace. The concentration of Hg was achieved through 40% HNO_3:HCl=2:1 (v/v) trapping solutions. The preconcentrated solutions were diluted to 0.5 ng/ml with an acid concentration of 10-20% for Hg isotope measurements using a Neptune Plus multi-collector inductively coupled plasma mass spectrometry (see also Yin et al., 2016a). External standard reference material GSS-4 (yellow soil) and method blanks were prepared in the same way as the samples. The Hg recoveries were 92%-103% for GSS-4, and Hg blanks were below 10 pg/mL. NIST-3177 secondary standard solutions, diluted to 0.5 ng/mL Hg with 10% HCl, were measured every 10 samples to ensure the instrument was working properly. Four core samples with Hg-isotope data were washed by DCM and processed with the same method above to explore the effect of DCM-washing on Hg-isotopes. All Hg-isotope analyses were carried out at the State Key Laboratory of Environmental Geochemistry, Institute of Geochemistry, Chinese Academy of Sciences, Guiyang.

Mass-dependent fractionation of Hg-isotopes is expressed as δ values in units of per mil (‰) by reference to bracketing NIST 3133 Hg standards analyzed before and after each sample following the convention proposed by Bergquist and Blum (2007):

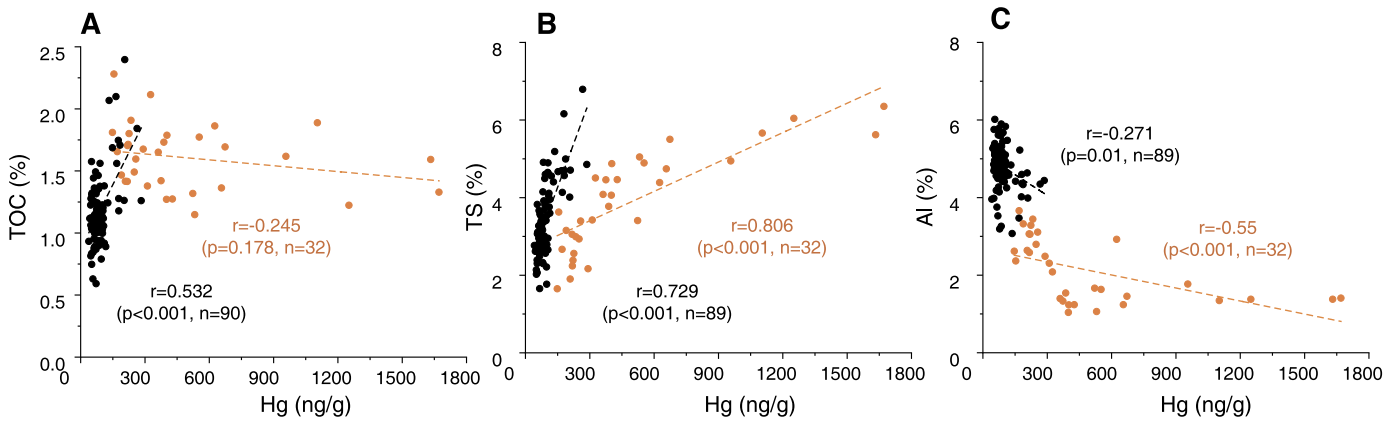

Fig. 3. Cross-plot of Hg versus total organic carbon (TOC), total sulfur (TS) and Al (a proxy for clay content) with linear correlation coefficients (Pearson r values) also shown. Orange points come from wet cuttings samples and black points are from core samples. See main text for details.

$$\delta^{202}Hg = [(^{202}Hg/^{198}Hg)_{samples}/(^{202}Hg/^{198}Hg)_{standard} - 1] \times 1000 \quad (1)$$

Mass-independent fractionation of Hg-isotopes is expressed in 'capital delta (Δ)' notation in units of per mil (‰) to quantify the difference between the measured δ^{xxx}Hg and the theoretically predicted δ^{xxx}Hg value:

$$\Delta^{199}Hg = \delta^{199}Hg - (0.252 \times \delta^{202}Hg) \quad (2)$$

$$\Delta^{201}Hg = \delta^{201}Hg - (0.752 \times \delta^{202}Hg) \quad (3)$$

The overall average and 2σ uncertainty of NIST-3177 (-0.53 ± 0.12‰, 0.00 ± 0.04‰ and -0.03 ± 0.05‰ for δ^{202}Hg, Δ^{199}Hg and Δ^{201}Hg, respectively, n = 5) and GSS-4 (-1.66 ± 0.14‰, -0.46 ± 0.02‰ and -0.43 ± 0.08‰ for δ^{202}Hg, Δ^{199}Hg and Δ^{201}Hg, respectively, n = 3) agree well with previous results (NIST-3177: -0.53 ± 0.10‰, -0.03 ± 0.04‰ and -0.02 ± 0.04‰ for δ^{202}Hg, Δ^{199}Hg and Δ^{201}Hg, respectively, n = 26, Yin et al., 2022. GSS-4: -1.67 ± 0.14‰, -0.34 ± 0.08‰, -0.35 ± 0.07‰ for δ^{202}Hg, Δ^{199}Hg and Δ^{201}Hg, respectively, n = 3, Sun et al., 2022).

3. Results

3.1. Assessing sample type/pre-treatment effects on Hg and Hg isotope data

The mean Hg content of raw core samples is 14.4 ng/g higher than the mean Hg content of de-oiled (i.e. DCM-washed) and decarbonated core samples (Table S3 in Supplementary Data). This mean difference is slightly larger than the precision (2σ) attained for Hg (2 ng/g) (Fig. S1). Nevertheless this difference is much lower than the mean difference observed between wet cuttings and core samples in the well (404 ng/g, Fig. 2).

For paired DCM-washed and raw core samples the mean difference in Δ^{199}Hg values is 0.03‰ (range: -0.06‰ to 0.02‰, Fig. S1). This average difference is within the combined uncertainty of the measurements (0.04‰). A paired t-test shows that there is no significant difference in Δ^{199}Hg between the raw samples and the 'de-oiled' samples ($p = 0.537$, $n = 4$). As suggested by Chen et al. (2022), the δ^{202}Hg values may be altered by the loss of lighter Hg-isotopes during metamorphism whereas the Δ^{199}Hg values are resistant to metamorphism (see also Deng et al., 2022). Thus, any thermal difference between the coring and drilling operations will not have affected the Δ^{199}Hg values.

3.2. Hg concentrations, TOC/TN and total sulfur

Hg concentrations through the 23/16b-9 well range from 42 ng/g to 1672 ng/g (Fig. 2). Hg contents prior to and during the onset of the PETM CIE (2848-2889.5 m) are relatively high (mean = 255 ng/g), with stable and lower values in the body of the CIE (2731-2848 m, mean = 95 ng/g). A return to relatively higher values occurs in the recovery of the CIE and above (2624-2731 m, mean = 689 ng/g, Fig. 2).

TOC and TOC/TN vary from 0.59% to 2.4% and from 5.67 to 19.4, respectively, with lower values during the CIE body and higher values towards the top of the studied interval (Fig. 2). Total sulfur (TS) in the well ranges from 1.65% to 6.79% (mean = 3.6%), and shows a gradually increasing trend throughout the studied interval.

3.3. Hg-isotopes

Hg-isotope mass-dependent fractionation values (MDF, δ^{202}Hg) range from -1.20‰ to 0.42‰ (mean = -0.35) (Table S2). We do not discuss δ^{202}Hg further in this study, however, given that δ^{202}Hg values are controlled by a variety of Hg-MDF processes and do not provide enough constraints on Hg sources (see also Section 1). By contrast, Hg-isotope mass-independent fractionation values (MIF, Δ^{199}Hg, see Section 2.3) can better fingerprint the source of Hg in marine sediments (e.g., terrestrial inputs versus atmospheric deposition of Hg^{II}) (see Section 1, Blum et al., 2014 and references therein). Δ^{199}Hg ranges from -0.3‰ to -0.09‰ (mean = -0.2‰, Fig. 2) in the samples. Δ^{199}Hg exhibits a long-term trend towards 0‰ from the base of the studied interval to ~2746.7 m. This trend is interrupted by a transient positive shift towards zero (0.14‰) within the onset of the PETM CIE (Fig. 2). Above 2746.7 m, Δ^{199}Hg is variable but exhibits an overall negative trend towards -0.3‰. These absolute values of Δ^{199}Hg are important for determining the source of Hg in the North Sea Basin, and the trends observed in the Δ^{199}Hg data can indicate changing sources/depositional pathways across the PETM as well. For all data in this study see Supplementary Data.

4. Discussion

4.1. Hg abundance and host phases

There is a strong correlation between Hg and TS through the well in both wet cuttings and core samples ($r = 0.729$, $p < 0.001$, $n = 89$ and $r = 0.806$, $p < 0.001$, $n = 32$, respectively, Fig. 3). There are weaker correlations between Hg and TOC ($r = -0.245$, $p = 0.178$, $n = 32$ and $r = 0.532$, $p < 0.001$, $n = 90$ for wet cuttings and core samples, respectively, Fig. 3). This suggests that the dominant host of Hg in the studied interval is sulfide, with a lesser hosting role played by organic matter (Shen et al., 2019b). Although clays can sometimes be an important host of Hg

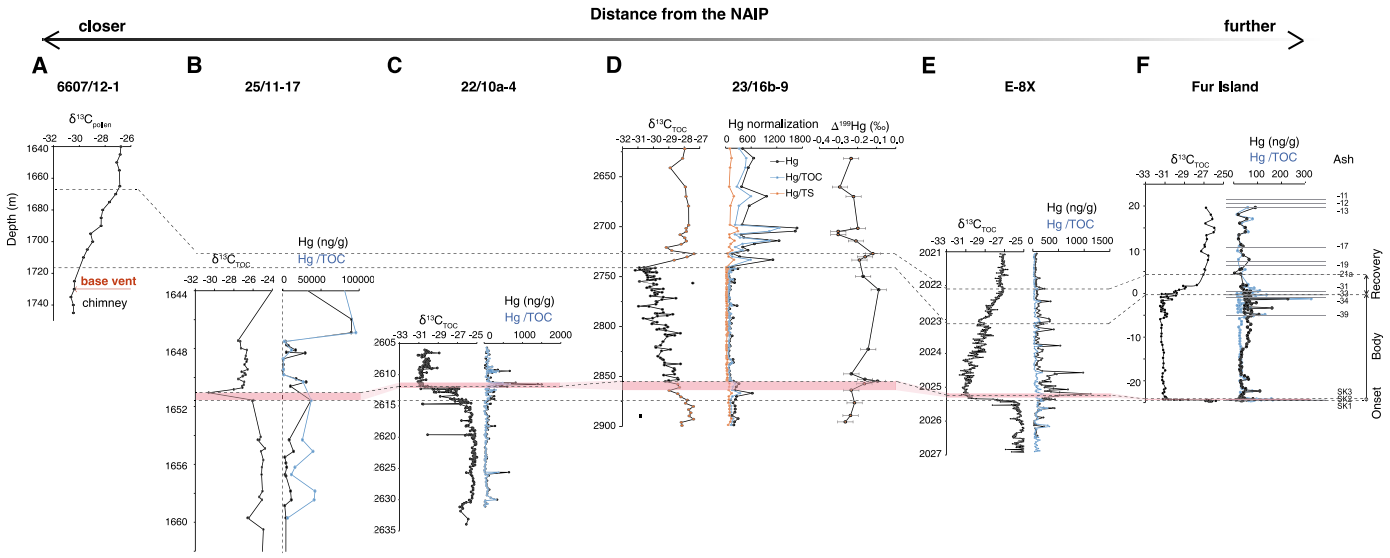

Fig. 4. Carbon-isotopes ($\delta^{13}C_{TOC}$ and $\delta^{13}C_{pollen}$), Hg abundance and Hg isotopes through the PETM from the North Sea Basin, ordered by the relative distance from the North Atlantic Igneous Province (NAIP). All depth/height scales in m. (A) well 6607/12-1 (Frieling et al., 2016). (B) well 25/11-17 (Grane field) (Jones et al., 2019). (C) well 22/10a-4 (Kender et al., 2021). (D) well 23/16b-9 (Jin et al., 2022 and this study). For interpretations of the different colored data in well 23/16b-9, see Fig. 2. (E) well E-8X (Kender et al., 2021). (F) Fur Island (Denmark, Jones et al., 2019), with prominent ash layers labeled as in Bøggild (1918) and Jones et al. (2019). Dashed lines are correlations between the sites based on the morphologies of the PETM carbon-isotope excursions (CIEs) (or parts thereof) observed at each site. Pink bar shows correlation of Hg data consistent with the CIE correlations. Base of the hydrothermal vent complex recognized by Frieling et al. (2016) is indicated in 6607/12-1.

(Shen et al., 2019a; Shen et al., 2020), Al (a proxy for clay content) has a negative correlation with Hg in the section ($r = -0.55$, $p < 0.001$, $n = 32$ and $r = -0.271$, $p = 0.01$, $n = 89$ for wet cuttings and core samples, respectively, Fig. 3).

The profiles of Hg/TS and Hg/TOC exhibit similar trends, and can be divided into 3 parts; with relatively high normalized Hg contents from 2848 to 2889.5 m, lower values from 2731 to 2848 m, and much higher values from 2624 to 2731 m. A similar pattern of Hg change through the PETM (i.e. relatively low Hg in the body of the CIE and higher concentrations below and above) has been observed in other sections in the North Sea Basin (e.g., well 25/11-17 and Fur Island, Jones et al., 2019, Fig. 4). When compared with existing Hg abundance data through the CIE from the North Sea Basin, our data emphasize a generally decreasing trend with increasing distance from the NAIP (Fig. 4), indicating a strong regionally controlled distribution of Hg in the North Sea Basin, as also noted in other studies (Jones et al., 2019; Tremblin et al., 2022).

4.2. Hg-isotope evidence for marked transient volcanism across the onset of the PETM

The slope of $\Delta^{199}Hg/\Delta^{201}Hg$ in well 23/16b-9 is 0.995 ± 0.16, which is consistent with photoreduction of aqueous Hg^{II} to Hg^0 ($\Delta^{199}Hg/\Delta^{201}Hg = 1.00 \pm 0.02$ (Bergquist and Blum, 2007), Fig. 5). The overall negative $\Delta^{199}Hg$ values in well 23/16b-9 suggest that the Hg is derived at least partly from terrestrial biomass (e.g., soil and vegetation). An abrupt positive excursion in $\Delta^{199}Hg$ (from $-0.23‰$ to $-0.09‰$) occurs just before the body of the PETM CIE within the onset interval, and is defined by both core and wet cuttings samples (Fig. 2, pink bar, see also Fig. 6A). Peaks in Hg/TS and Hg/TOC also occur within the onset interval (Fig. 2). Although limited sample resolution makes precise definition of the onset and body of the PETM in 23/16b-9 difficult, we note that within the resolution of the available data, broadly coeval Hg anomalies occur in nearby wells 22/10a-4 and E-8X (Fig. 4, pink bar). This shift towards zero $\Delta^{199}Hg$ values contemporaneous with relatively high Hg suggests a transient increase in volcanically derived Hg entering surface waters in the North Sea Basin with near-zero

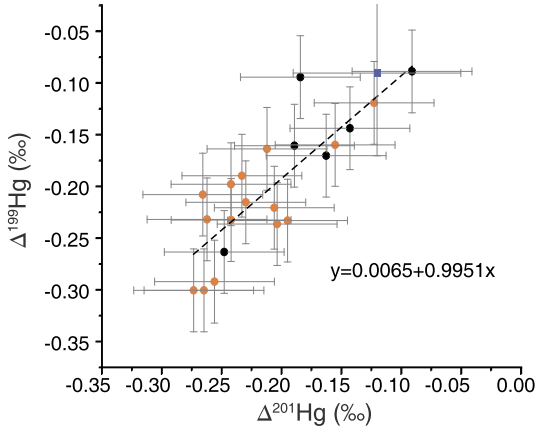

Fig. 5. Cross-plot of $\Delta^{199}Hg$ and $\Delta^{201}Hg$ (with analytical error bars). This plot highlights a linear trend that is consistent with photoreduction of aqueous Hg^{II} (idealized $\Delta^{199}Hg/\Delta^{201}Hg = 1.00 \pm 0.02$, Bergquist and Blum, 2007). The slope in this study is 0.995 ± 0.16. Orange points come from wet cuttings samples and black points are from core samples. Blue square is from Gleason et al. (2017) from Lomonosov Ridge.

$\Delta^{199}Hg$. Ostensibly, the transient positive shift of $\Delta^{199}Hg$ could also have arisen due to a short-lived reduction in terrestrial input. However, TOC/TN values (a broad proxy for organic matter type, e.g. Meyers, 1994; Fig. S2) do not show any changes consistent with reduced terrestrial input, and indeed there is no significant correlation between $\Delta^{199}Hg$ and TOC/TN across the entire record (Fig. S2). Moreover, the inference of a short-lived phase of extrusive volcanism across the PETM onset is further supported by osmium-isotope data (Schmitz et al., 2004; Wieczorek et al., 2013; Dickson et al., 2015). Notably, in Kheu River (Georgia), Guru Fatima (Tajikistan) and Zumaya (Spain) sections, there is a transient decrease in $^{187}Os/^{188}Os_{initial}$ broadly coeval within the onset of the PETM and our positive excursion of $\Delta^{199}Hg$ (Fig. 6). This decrease is interpreted to reflect the input of unradiogenic (i.e. low $^{187}Os/^{188}Os_{initial}$) Os from weathering of fresh basalts (Dickson et al., 2015). In addition, this postulated input of volcanogenic Hg may correspond to an ash layer (SK3) in Fur Island (Denmark)

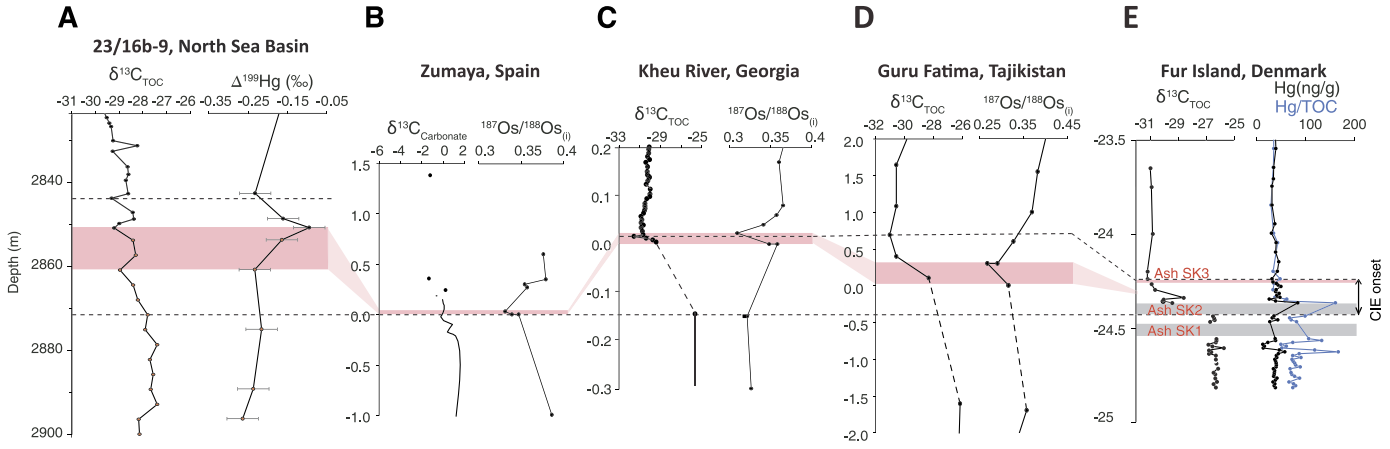

Fig. 6. Carbon-isotope ($\delta^{13}C_{TOC}$) data and geochemical proxies that support enhanced volcanism within the onset of the PETM CIE. (A) Carbon-isotope and $\Delta^{199}Hg$ data in well 23/16b-9 (Jin et al., 2022 and this study). (B) Carbon-isotope and Os-isotope data from Zumaya, Spain (Schmitz et al., 2004). (C) and (D) Carbon-isotope and Os-isotope data from Kheu River (Georgia) and Guru Fatima (Tajikistan) (Dickson et al., 2015). (E) Carbon-isotope, Hg abundance and Hg/TOC data from Fur Island, Denmark with ash layers also labeled (as in Jones et al., 2019). In B, C and D, the shifts towards lower $^{187}Os/^{188}Os_{initial}$ in the shaded pink interval are interpreted to reflect a transient input of unradiogenic Os from the weathering of fresh basalts (Dickson et al., 2015). Pink bar shows inferred correlation of the volcanism proxies consistent with the CIE onset correlations.

based on the correlation of the carbon-isotopes in both sections (Jones et al., 2019; Fig. 6E).

4.3. Evidence for sustained magmatic activity through the body of the PETM

The inferred volcanogenic Hg pulse within the onset of the PETM interrupts a more protracted increase of 0.17‰ in $\Delta^{199}Hg$ that spans from the base of the studied interval (2889.5 m, below the CIE) to 2746.7 m (within the body of the CIE) (Fig. 2). This trend can be interpreted to reflect a long-term input of volcanogenic Hg against a background of dominantly terrestrially-derived Hg, an inference supported by the broad age constraints available for NAIP volcanism (Wotzlaw et al., 2012; Wilkinson et al., 2017; Kasbohm et al., 2021) and the volcanic sequences spanning the Paleocene-Eocene boundary from Rockall Plateau (Gernon et al., 2022). This protracted positive trend, however, does not correspond to consistently elevated Hg abundance, as would typically be expected during an interval of increased volcanism. Indeed Hg, Hg/TOC and Hg/TS decrease sharply close to the end of the transient positive $\Delta^{199}Hg$ excursion at ~2848 m and remain low throughout the body of the CIE until 2731 m (Fig. 2). This long-term positive trend could thus instead have resulted from decreased soil Hg input, possibly related to rising global sea level through the PETM (Sluijs et al., 2008). However, as already noted above in Section 4.2, there is no significant correlation between $\Delta^{199}Hg$ and TOC/TN through the studied succession (Fig. S2), suggesting that any changes in the relative abundance of marine and terrestrial components were unlikely to have played a significant role in influencing the $\Delta^{199}Hg$ signal. Strictly, in the CIE body interval there are not enough data points to resolve any correlation between $\Delta^{199}Hg$ and TOC/TN. However, there is no decreasing trend in TOC/TN in the CIE body coeval with rising $\Delta^{199}Hg$ (as might be expected if terrestrial fluxes were falling). Thus, rising sea level likely had little influence on the trend towards higher $\Delta^{199}Hg$ values through the body of the PETM.

The relatively low Hg, Hg/TOC and Hg/TS within the body of the CIE between 2731 m and 2848 m (Fig. 4D) is coincident with a ~10-fold increase in sedimentation rate in the well (Jin et al., 2022), and there is a positive correlation between Hg and TOC/TN in this part of the well ($r = 0.404$, $p < 0.001$, $n = 90$, Fig. S2). Hg drawdown potential in this interval could thus have been limited owing to reduced TOC caused by sediment dilution (Wang et al., 2018). However, reduction of both Hg and TOC in this way would leave Hg/TOC ratios relatively unaffected, but Hg/TOC also decreases (Fig. 2). Similarly, despite the increase in sedimentation rates palynology data indicate no evidence of large-scale terrestrial input, and significant sediment reworking is not apparent based on the recovered flora from either this or nearby wells (Vieira and Jolley, 2020; Vieira et al., 2020; Jolley et al., 2022). Taken together, these observations mean that it is unlikely that sediment reworking and sediment dilution was a cause for the low Hg. One possibility then is that an increased portion of marine organic matter from algal sources (with lower TOC/TN, Meyers, 1994) was triggered by increased nutrient delivery associated with enhanced freshwater fluxes from land (see, for example, Osleger et al., 2009). An increased proportion of algal matter in this part of the well has been noted previously (Jolley et al., 2022). Relative to terrestrial organic matter, this marine organic matter likely has a lower affinity for Hg (Percival et al., 2015, 2018), and thus this might have contributed to the lower normalized Hg values in the CIE body – albeit without significant influence on $\Delta^{199}Hg$ (Fig. S2).

A further possibility is that the sharp decrease in Hg abundance through the body of the CIE is due at least in part to the contrasting sample types analyzed (wet cuttings and core samples). Notably, core samples have markedly lower Hg and TOC/TN compared to wet cuttings samples (Fig. 2), and Hg and TOC/TN correlate only within the cored interval of the well (Fig. S2). Although this may point to an issue related to the sample type, as noted earlier a similar pattern of Hg change (i.e. relatively low Hg in the body of the CIE and higher concentrations below and above) has been observed previously in nearby sections (well 25/11-17 and Fur Island, Jones et al., 2019, Fig. 4). Although the PETM interval is poorly defined in well 25/11-17 (Fig. 4), sedimentation rates likely increased across the PETM at these two sites as well (Jones et al., 2019). Equally, as noted in Section 3.1, the experiments conducted to replicate the sample treatment (DCM-washing) used in the preparation of wet cuttings samples suggests that sample preparation was not a cause of the observed differences (Fig. S1).

Regardless of the specific controls on Hg abundance within the CIE body, the trend towards higher $\Delta^{199}Hg$ from the base of the studied interval to 2746.7 m suggests a protracted interval of volcanism. The possible influence of sample type on the Hg-isotope data and this interpretation can be ruled out because: 1) there is no significant difference in $\Delta^{199}Hg$ between core and wet cuttings samples within the CIE (t-test, $p = 0.42$), 2) the transient increase

in Δ^{199}Hg within the onset interval attributable to marked transient volcanism is defined by both wet cuttings and core samples (Fig. 2, see also Fig. 6A), 3) experiments indicate that the different sample preparation of wet cuttings and core samples have no measurable effect on Δ^{199}Hg (see Section 3.1, Fig. S1), and 4) despite the volatility of Hg recent work has emphasized the robustness of Hg-isotopes to any temperature differences between coring and drilling operations (Chen et al., 2022; Deng et al., 2022, see Section 3.1).

Our Hg-isotope evidence for sustained volcanism through the CIE body of the PETM is supported by carbon cycle modeling studies, which have indicated that a single initial carbon input is unable to reconstruct the long duration of the PETM (Zeebe et al., 2009; Zeebe, 2013; see also Frieling et al., 2016). Thus, sustained magmatism may thus have played a key role in controlling the relatively long duration (~160,000 years, Jin et al., 2022 and references therein) of the CIE body.

4.4. Hg-isotope signals across the end of the PETM

Above 2746.7 m, Δ^{199}Hg values begin a long-term decrease, just prior to the start of the recovery of the CIE, and likely reflecting a relative reduction in volcanogenic Hg flux relative to terrestrial inputs. This long-term negative trend in Δ^{199}Hg approximately corresponds to an overall increase in Hg, Hg/TS and Hg/TOC above 2746.7 m. In detail, the negative trend in Δ^{199}Hg above 2746.7 m is quite variable (Fig. 2H). Hg/TS ratios are also variable over this interval, with marked transient increases in Hg/TS occurring between ~2670 m and ~2731 m, and with the largest increase (~2703 m) broadly coeval with the most negative Δ^{199}Hg values in the succession (Fig. 2G, all in wet cuttings samples). As noted earlier, Svensen et al. (2004) proposed that the intrusion of mantle-derived melts into organic carbon-rich sediments (and consequent CH_4 release) at hydrothermal vent complexes in the Norwegian Sea may have occurred during the PETM (see also Gutjahr et al., 2017). The Δ^{199}Hg of the Hg liberated from organic-rich sediments in this way would likely be negative based on data from coals, peats, and black shales (Yin et al., 2016b; Shen et al., 2022b), and unaffected by extreme heating (Chen et al., 2022; Deng et al., 2022). As such, Hg sourced from episodic explosive hydrothermal venting could have been a contributory cause of the observed negative shifts in Δ^{199}Hg and the high and variable relative Hg abundance above 2746.7 m. Extremely high Hg contents towards the end of the CIE and after have also been noted in well 25/11-17 (up to 90,100 ng/g, Jones et al., 2019, Fig. 4). Although precise correlation with 23/16b-9 is difficult (Fig. 4), Jones et al. (2019) noted that such extreme values are hard to explain without invoking a major release of Hg from a proximal hydrothermal or perhaps submarine volcanic source.

Direct evidence for hydrothermal venting coeval with the CIE recovery and in younger strata is lacking. From a single record from the Vøring Basin, Frieling et al. (2016) showed that the base of a hydrothermal vent complex where explosive venting may have occurred is located just below the start of the CIE recovery (Fig. 4A), but that venting was likely restricted to the CIE body (Frieling et al., 2016). Explosive hydromagmatic volcanism in shallow subaqueous environments from the NAIP is, however, recorded across the CIE recovery and well into the Eocene (Stokke et al., 2020; see also Jones et al., 2019). We also note that at some sites deposited close to or far away from the NAIP, such as in well E_8X, Spain and the New Jersey coastal plain, there is negligible evidence for volcanism after the CIE (Jones et al., 2019; Liu et al., 2019; Kender et al., 2021; Tremblin et al., 2022). Taken together, these observations highlight the likely complexity of NAIP magmatic activity and the expression of this activity in both Hg abundance and Hg-isotope records. Indeed, recent work has implicated carbon released from decompression melting of entrained subcontinental lithospheric mantle along the northeast Atlantic rift axis as a trigger of the PETM (Gernon et al., 2022). Ultimately, the precise source(s) of carbon or locus of any outgassing using Hg-isotope data are difficult to distinguish on the basis of Hg-isotope data alone (Yin et al., 2022).

5. Conclusions

Our study provides the first Hg-isotope evidence of a causal link between large igneous province emplacement and the PETM. Notably, our work supports a temporal link between CO_2 release from volcanic activity and the initiation of the event. Elevated volcanogenic Hg fluxes, and hence also CO_2 fluxes, likely persisted through most of the PETM in the North Sea Basin. Taken together, our data can explain both the triggering mechanism and long duration of the PETM. Towards the end of, and after, the PETM the data suggest an overall waning influence of direct volcanogenic Hg outgassing. Our Hg-isotope data augment previous studies that analyzed Hg abundance only, and which also provided evidence for enhanced volcanism within the PETM onset. At the same time, our new work demonstrates how Hg abundance data alone may be insufficient to fully validate volcanism in some sedimentary settings, particularly with changing environmental conditions that can affect the relative abundance of Hg. Equally, large variations among published Hg abundance data emphasize the strong regional controls on Hg deposition. Our work helps to validate the use of Hg-isotopes as an important tool for assessing the role of volcanism in driving large-scale environmental change. Nevertheless, the precise interpretation of these data remains difficult, particularly in the context of robustly assessing magmatic styles and Hg sources. Further Hg-isotope work across the PETM is now needed to assess the possible regional controls on Hg-isotope signals close to the NAIP.

CRediT authorship contribution statement

Simin Jin: conceived and designed the study, led the laboratory work, data analysis, writing and editing of the manuscript.

David B. Kemp: conceptualized, supervised and funded the study, data analysis, reviewing and editing.

Runsheng Yin: measured Hg-isotopes, data analysis, reviewing and editing.

Ruiyang Sun: measured Hg-isotopes, data analysis.

Jun Shen: measured Hg concentrations, data analysis, reviewing and editing.

David W. Jolley: provided study materials, data analysis, reviewing and editing.

Manuel Vieira: provided study materials, reviewing and editing.

Chunju Huang: data analysis, reviewing and editing.

Declaration of competing interest

The authors declare that they have no known competing financial interests or personal relationships that could have appeared to influence the work reported in this paper.

Data availability

Data will be made available on request.

Acknowledgements

We thank the two anonymous reviewers for their valuable suggestions that helped us to improve the quality of this paper. This work was supported by the National Natural Science Foundation

of China (Grant No. 41888101, 42230208, 42172039), National Recruitment Program for Young Professionals (P.R. China) to DBK and the National Key R&D Program of China (2022YFF0802900). We thank Shell UK and partners for their support and permission to publish this research. We also thank Di Chen for assistance with laboratory work. This work is a contribution to IGCP739.

Appendix A. Supplementary material

Supplementary material related to this article can be found online at https://doi.org/10.1016/j.epsl.2022.117926.

References

Bond, D.P., Grasby, S.E., 2017. On the causes of mass extinctions. Palaeogeogr. Palaeoclimatol. Palaeoecol. 478, 3–29.
Bergquist, B.A., Blum, J.D., 2007. Mass-dependent and-independent fractionation of Hg isotopes by photoreduction in aquatic systems. Science 318 (5849), 417–420.
Blum, J.D., Sherman, L.S., Johnson, M.W., 2014. Mercury isotopes in earth and environmental sciences. Annu. Rev. Earth Planet. Sci. 42, 249–269.
Bøggild, O.B., 1918. Den vulkanske Aske i Moleret samt en Oversigt over Danmarks ældre Tertiærbjergarter. Bull. Geol. Soc. Den. 33, 1–159.
Charbonnier, G., Morales, C., Duchamp-Alphonse, S., Westermann, S., Adatte, T., Föllmi, K.B., 2017. Mercury enrichment indicates volcanic triggering of Valanginian environmental change. Sci. Rep. 7, 40808.
Chen, D., Ren, D., Deng, C., Tian, Z., Yin, R., 2022. Mercury loss and isotope fractionation during high-pressure and high-temperature processing of sediments: Implication for the behaviors of mercury during metamorphism. Geochim. Cosmochim. Acta 334, 231–240.
Demers, J.D., Blum, J.D., Zak, D.R., 2013. Mercury isotopes in a forested ecosystem: implications for air-surface exchange dynamics and the global mercury cycle. Glob. Biogeochem. Cycles 27 (1), 222–238.
Deng, C., Geng, H., Xiao, T., Chen, D., Sun, G., Yin, R., 2022. Mercury isotopic compositions of the Precambrian rocks and implications for tracing mercury cycling in Earth's interior. Precambrian Res. 373, 106646.
Dickens, G.R., O'Neil, J.R., Rea, D.K., Owen, R.M., 1995. Dissociation of oceanic methane hydrate as a cause of the carbon isotope excursion at the end of the Paleocene. Paleoceanography 10 (6), 965–971.
Dickson, A.J., Cohen, A.S., Coe, A.L., Davies, M., Shcherbinina, E.A., Gavrilov, Y.O., 2015. Evidence for weathering and volcanism during the PETM from Arctic Ocean and Peri-Tethys osmium isotope records. Palaeogeogr. Palaeoclimatol. Palaeoecol. 438, 300–307.
Frieling, J., Svensen, H.H., Planke, S., Cramwinckel, M.J., Selnes, H., Sluijs, A., 2016. Thermogenic methane release as a cause for the long duration of the PETM. Proc. Natl. Acad. Sci. 113 (43), 12059–12064.
Gernon, T.M., Barr, R., Fitton, J.G., Hincks, T.K., Keir, D., Longman, J., Merdith, A.S., Mitchell, R.N., Palmer, M.R., 2022. Transient mobilization of subcrustal carbon coincident with Palaeocene–Eocene Thermal Maximum. Nat. Geosci. 15 (7), 573–579.
Gleason, J.D., Blum, J.D., Moore, T.C., Polyak, L., Jakobsson, M., Meyers, P.A., Biswas, A., 2017. Sources and cycling of mercury in the paleo Arctic Ocean from Hg stable isotope variations in Eocene and Quaternary sediments. Geochim. Cosmochim. Acta 197, 245–262.
Grasby, S.E., Shen, W., Yin, R., Gleason, J.D., Blum, J.D., Lepak, R.F., Hurley, J.P., Beauchamp, B., 2017. Isotopic signatures of mercury contamination in latest Permian oceans. Geology 45 (1), 55–58.
Grasby, S.E., Them II, T.R., Chen, Z., Yin, R., Ardakani, O.H., 2019. Mercury as a proxy for volcanic emissions in the geologic record. Earth-Sci. Rev. 196, 102880.
Gratz, L.E., Keeler, G.J., Blum, J.D., Sherman, L.S., 2010. Isotopic composition and fractionation of mercury in Great Lakes precipitation and ambient air. Environ. Sci. Technol. 44 (20), 7764–7770.
Gutjahr, M., Ridgwell, A., Sexton, P.F., Anagnostou, E., Pearson, P.N., Pälike, H., Norris, R.D., Foster, G.L., 2017. Very large release of mostly volcanic carbon during the Palaeocene-Eocene Thermal Maximum. Nature 548 (7669), 573–577.
Jin, S., Kemp, D.B., Jolley, D.W., Vieira, M., Zachos, J.C., Huang, C., Li, M., Chen, W., 2022. Large-scale, astronomically paced sediment input to the North Sea Basin during the Paleocene Eocene Thermal Maximum. Earth Planet. Sci. Lett. 579, 117340.
Jolley, D.W., Millett, J.M., Schofield, N., Broadley, L., 2021. Stratigraphy of volcanic rock successions of the North Atlantic rifted margin: the offshore record of the Faroe–Shetland and Rockall basins. Earth Environ. Sci. Trans. R. Soc. Edinb. 112 (2), 61–88.
Jolley, D., Vieira, M., Jin, S., Kemp, D., 2022. Palynofloras, paleoenvironmental change and the inception of the Paleocene Eocene Thermal Maximum; the record of the Forties Fan, Sele Formation, North Sea Basin. J. Geol. Soc. jgs2021-131.
Jones, M.T., Percival, L.M., Stokke, E.W., Frieling, J., Mather, T.A., Riber, L., Schubert, B.A., Schultz, B., Tegner, C., Planke, S., Svensen, H.H., 2019. Mercury anomalies across the Palaeocene–Eocene thermal maximum. Clim. Past 15 (1), 217–236.
Kasbohm, J., Schoene, B., Burgess, S., 2021. Radiometric constraints on the timing, tempo, and effects of large igneous province emplacement. In: Ernst, R.E., et al. (Eds.), Large Igneous Provinces: A Driver of Global Environmental and Biotic Changes. In: AGU Geophysical Monograph, vol. 255, pp. 25–80.
Keller, G., Mateo, P., Punekar, J., Khozyem, H., Gertsch, B., Spangenberg, J., Bitchong, A.M., Adatte, T., 2018. Environmental changes during the Cretaceous-Paleogene mass extinction and Paleocene-Eocene thermal maximum: implications for the Anthropocene. Gondwana Res. 56, 69–89.
Kender, S., Bogus, K., Pedersen, G.K., Dybkjær, K., Mather, T.A., Mariani, E., Ridgwell, A., Riding, J.B., Wagner, T., Hesselbo, S.P., Leng, M.J., 2021. Paleocene/Eocene carbon feedbacks triggered by volcanic activity. Nat. Commun. 12, 5186.
Liu, Z., Horton, D.E., Tabor, C., Sageman, B.B., Percival, L.M., Gill, B.C., Selby, D., 2019. Assessing the contributions of comet impact and volcanism toward the climate perturbations of the Paleocene-Eocene thermal maximum. Geophys. Res. Lett. 46 (24), 14798–14806.
Meyers, P.A., 1994. Preservation of elemental and isotopic source identification of sedimentary organic matter. Chem. Geol. 114, 289–302.
Osleger, D.A., Heyvaert, A.C., Stoner, J.S., Verosub, K.L., 2009. Lacustrine turbidites as indicators of Holocene storminess and climate: Lake Tahoe, California and Nevada. J. Paleolimnol. 42 (1), 103–122.
Penman, D.E., Hönisch, B., Zeebe, R.E., Thomas, E., Zachos, J.C., 2014. Rapid and sustained surface ocean acidification during the Paleocene-Eocene Thermal Maximum. Paleoceanography 29 (5), 357–369.
Percival, L.M.E., Witt, M.L.I., Mather, T.A., Hermoso, M., Jenkyns, H.C., Hesselbo, S.P., Al-Suwaidi, A.H., Storm, M.S., Xu, W., Ruhl, M., 2015. Globally enhanced mercury deposition during the end-Pliensbachian extinction and Toarcian OAE: a link to the Karoo–Ferrar Large Igneous Province. Earth Planet. Sci. Lett. 428, 267–280.
Percival, L.M.E., Jenkyns, H.C., Mather, T.A., Dickson, A.J., Batenburg, S.J., Ruhl, M., Hesselbo, S.P., Barclay, R., Jarvis, I., Robinson, S.A., Woelders, L., 2018. Does large igneous province volcanism always perturb the mercury cycle? Comparing the records of Oceanic Anoxic Event 2 and the end-Cretaceous to other Mesozoic events. Am. J. Sci. 318 (8), 799–860.
Pyle, D.M., Mather, T.A., 2003. The importance of volcanic emissions for the global atmospheric mercury cycle. Atmos. Environ. 37 (36), 5115–5124.
Ravichandran, M., 2004. Interactions between mercury and dissolved organic matter—-a review. Chemosphere 55 (3), 319–331.
Sanei, H., Grasby, S.E., Beauchamp, B., 2012. Latest Permian mercury anomalies. Geology 40 (1), 63–66.
Saunders, A.D., Fitton, J.G., Kerr, A.C., Norry, M.J., Kent, R.W., 1997. The north Atlantic igneous province. In: Mahoney, J.J., Coffin, M.F. (Eds.), Large Igneous Provinces. In: Geophysical Monograph, vol. 100. American Geophysical Union, pp. 45–93.
Schmitz, B., Peucker-Ehrenbrink, B., Heilmann-Clausen, C., Åberg, G., Asaro, F., Lee, C.T.A., 2004. Basaltic explosive volcanism, but no comet impact, at the Paleocene–Eocene boundary: high-resolution chemical and isotopic records from Egypt, Spain and Denmark. Earth Planet. Sci. Lett. 225 (1–2), 1–17.
Schofield, N., Jolley, D., Holford, S., Archer, S., Watson, D., Hartley, A., Hartley, J., Muirhead, D., Underhill, J., Green, P., 2018. Challenges of future exploration within the UK Rockall Basin. In: Geological Society. London. In: Petroleum Geology Conference Series, vol. 8(1). Geological Society of London, pp. 211–229.
Selin, N.E., 2009. Global biogeochemical cycling of mercury: a review. Ann. Rev. Environ. Res. 34, 43–63.
Sun, R., Yao, H., Deng, C., Grasby, S.E., Wang, C., Chen, X., Yin, R., 2022. Volcanism-triggered climatic control on Late Cretaceous oceans. Geochem. Geophys. Geosyst. 23, e2021GC010292.
Shen, J., Chen, J., Algeo, T.J., Yuan, S., Feng, Q., Yu, J., Zhou, L., O`Connell, B., Planavsky, N.J., 2019a. Evidence for a prolonged Permian-Triassic extinction interval from global marine mercury records. Nat. Commun. 10, 1563.
Shen, J., Algeo, T.J., Chen, J., Planavsky, N.J., Feng, Q.L., Yu, J.X., Liu, J.L., 2019b. Mercury in marine Ordovician/Silurian boundary sections of South China is sulfide hosted and non-volcanic in origin. Earth Planet. Sci. Lett. 511, 130–140.
Shen, J., Feng, Q., Algeo, T.J., Liu, J., Zhou, C., Wei, W., Liu, J., Them II, T.R., Gill, B.C., Chen, J., 2020. Sedimentary host phases of mercury (Hg) and implications for use of Hg as a volcanic proxy. Earth Planet. Sci. Lett. 543, 116333.
Shen, J., Yin, R., Zhang, S., Algeo, T.J., Bottjer, D.J., Yu, J.X., Xu, G.Z., Penman, D., Wang, Y.D., Li, L.Q., Shi, X., Planavsky, N.J., Feng, Q.L., Xie, S.C., 2022a. Intensified continental chemical weathering and carbon-cycle perturbations linked to volcanism during the Triassic–Jurassic transition. Nat. Commun. 13, 299.
Shen, J., Yin, R., Algeo, T.J., Svensen, H.H., Schoepfer, S.D., 2022b. Mercury evidence for combustion of organic-rich sediments during the end-Triassic crisis. Nat. Commun. 13, 1307.
Sial, A.N., Chen, J., Lacerda, L.D., Frei, R., Tewari, V.C., Pandit, M.K., Gaucher, C., Ferreira, V.P., Cirilli, S., Peralta, S., Korte, C., Barbosa, J.A., Pereira, N.S., 2016. Mercury enrichment and Hg isotopes in Cretaceous–Paleogene boundary successions: links to volcanism and palaeoenvironmental impacts. Cretac. Res. 66, 60–81.
Sluijs, A., Brinkhuis, H., Schouten, S., Bohaty, S.M., John, C.M., Zachos, J.C., Reichart, G., Sinninghe Damste, J.S., Crouch, E.M., Dickens, G.R., 2007. Environmental precursors to rapid light carbon injection at the Palaeocene/Eocene boundary. Nature 450 (7173), 1218–1221.
Sluijs, A., Brinkhuis, H., Crouch, E.M., John, C.M., Handley, L., Munsterman, D., Bohaty, S.M., Zachos, J.C., Reichart, G.J., Shouten, S., Pancost, R.D., Sinninghe Damsté, J.S.,

Welters, N.L.D., Lotter, A.F., Dickens, G.R., 2008. Eustatic variations during the Paleocene-Eocene greenhouse world. Paleoceanography 23, PA4216.
Stephenson, M.H., Leng, M.J., Vane, C.H., Osterloff, P.L., Arrowsmith, C., 2005. Investigating the record of Permian climate change from argillaceous sedimentary rocks, Oman. J. Geol. Soc. 162 (4), 641–651.
Stokke, E.W., Liu, E., Jones, M.T., 2020. Evidence of explosive hydromagmatic eruptions during the emplacement of the North Atlantic Igneous Province. Volcanica 3 (2), 227–250.
Storey, M., Duncan, R.A., Tegner, C., 2007. Timing and duration of volcanism in the North Atlantic Igneous Province: implications for geodynamics and links to the Iceland hotspot. Chem. Geol. 241 (3–4), 264–281.
Svensen, H., Planke, S., Malthe-Sørenssen, A., Jamtveit, B., Myklebust, R., Rasmussen Eidem, T., Rey, S.S., 2004. Release of methane from a volcanic basin as a mechanism for initial Eocene global warming. Nature 429 (6991), 542–545.
Svensen, H., Planke, S., Corfu, F., 2010. Zircon dating ties NE Atlantic sill emplacement to initial Eocene global warming. J. Geol. Soc. 167 (3), 433–436.
Thibodeau, A.M., Ritterbush, K., Yager, J.A., West, A.J., Ibarra, Y., Bottjer, D.J., Berelson, W.M., Bergquist, B.A., Corsetti, F.A., 2016. Mercury anomalies and the timing of biotic recovery following the end-Triassic mass extinction. Nat. Commun. 7, 11147.
Thomas, E., 1989. Development of Cenozoic deep-sea benthic foraminiferal faunas in Antarctic waters. Geol. Soc. (Lond.) Spec. Publ. 47 (1), 283–296.
Tremblin, M., Khozyem, H., Adatte, T., Spangenberg, J.E., Fillon, C., Grauls, A., Hunger, T., Nowak, A., Läuchli, C., Lasseur, E., Roig, J.Y., Serrano, O., Calassou, S., Guillocheau, F., Castelltort, S., 2022. Mercury enrichments of the Pyrenean foreland basins sediments support enhanced volcanism during the Paleocene-Eocene thermal maximum (PETM). Glob. Planet. Change 212, 103794.
Vieira, M., Mahdi, S., Holmes, N., 2020. High resolution biostratigraphic zonation for the UK central North Sea Paleocene. Mar. Pet. Geol. 117, 104400.
Vieira, M., Jolley, D., 2020. Stratigraphic and spatial distribution of palynomorphs in deep water turbidites: a meta-data study from the UK Central North Sea Paleogene. Mar. Pet. Geol. 122, 104638.
Wang, X., Cawood, P.A., Zhao, H., Zhao, L., Grasby, S.E., Chen, Z.Q., Wignall, P.B., Lv, Z., Han, C., 2018. Mercury anomalies across the end Permian mass extinction in South China from shallow and deep water depositional environments. Earth Planet. Sci. Lett. 496, 159–167.
Wieczorek, R., Fantle, M.S., Kump, L.R., Ravizza, G., 2013. Geochemical evidence for volcanic activity prior to and enhanced terrestrial weathering during the Paleocene Eocene Thermal Maximum. Geochim. Cosmochim. Acta 119, 391–410.
Wilkinson, C.M., Ganerød, M., Hendriks, B.W., Eide, E.A., 2017. Compilation and appraisal of geochronological data from the North Atlantic Igneous Province (NAIP). Geol. Soc. (Lond.) Spec. Publ. 447 (1), 69–103.
Wotzlaw, J.F., Bindeman, I.N., Schaltegger, U., Brooks, C.K., Naslund, H.R., 2012. High-resolution insights into episodes of crystallization, hydrothermal alteration and remelting in the Skaergaard intrusive complex. Earth Planet. Sci. Lett. 355, 199–212.
Yin, R., Krabbenhoft, D.P., Bergquist, B.A., Zheng, W., Lepak, R.F., Hurley, J.P., 2016a. Effects of mercury and thallium concentrations on high precision determination of mercury isotopic composition by Neptune Plus multiple collector inductively coupled plasma mass spectrometry. J. Anal. At. Spectrom. 31 (10), 2060–2068.
Yin, R., Feng, X., Hurley, J.P., Krabbenhoft, D.P., Lepak, R.F., Hu, R., Zhang, Q., Li, Z., Bi, X., 2016b. Mercury isotopes as proxies to identify sources and environmental impacts of mercury in sphalerites. Sci. Rep. 6, 18686.
Yin, R., Chen, D., Pan, X., Deng, C., Chen, L., Song, X., Yu, S., Zhu, C., Wei, X., Xu, Y., Feng, X., Blum, J.D., Lehmann, B., 2022. Mantle Hg isotopic heterogeneity and evidence of oceanic Hg recycling into the mantle. Nat. Commun. 13 (1), 948.
Zachos, J.C., Wara, M.W., Bohaty, S., Delaney, M.L., Petrizzo, M.R., Brill, A., Bralower, T.J., Premoli-Silva, I., 2003. A transient rise in tropical sea surface temperature during the Paleocene-Eocene thermal maximum. Science 302 (5650), 1551–1554.
Zachos, J.C., Röhl, U., Schellenberg, S.A., Sluijs, A., Hodell, D.A., Kelly, D.C., Thomas, E., Nicolo, M., Raffi, I., Lourens, L.J., Mccarren, H., Kroon, D., 2005. Rapid acidification of the ocean during the Paleocene-Eocene thermal maximum. Science 308 (5728), 1611–1615.
Zambardi, T., Sonke, J.E., Toutain, J.P., Sortino, F., Shinohara, H., 2009. Mercury emissions and stable isotopic compositions at Vulcano Island (Italy). Earth Planet. Sci. Lett. 277 (1–2), 236–243.
Zeebe, R.E., Zachos, J.C., Dickens, G.R., 2009. Carbon dioxide forcing alone insufficient to explain Palaeocene–Eocene Thermal Maximum warming. Nat. Geosci. 2 (8), 576–580.
Zeebe, R.E., 2013. What caused the long duration of the Paleocene-Eocene Thermal Maximum? Paleoceanography 28 (3), 440–452.

Further reading

Sonke, J.E., 2011. A global model of mass independent mercury stable isotope fractionation. Geochim. Cosmochim. Acta 75 (16), 4577–4590.